Advanced sensing and imaging for efficient energy exploration in complex reservoirs

Nasser Kazemi, Siavash Nejadi, Jean Auriol, Jordan Curkan, Roman J Shor, Kristopher A Innanen, Stephen M Hubbard, Ian D Gates

Energy Reports xxx (xxxx) xxx

Contents lists available at ScienceDirect

Energy Reports

journal homepage: www.elsevier.com/locate/egyr

Advanced sensing and imaging for efficient energy exploration in complex reservoirs

Nasser Kazemi [a,*], Siavash Nejadi [a], Jean Auriol [b], Jordan Curkan [a], Roman J. Shor [a], Kristopher A. Innanen [a], Stephen M. Hubbard [a], Ian D. Gates [a]

[a] University of Calgary, Canada
[b] Université Paris Saclay, France

ARTICLE INFO

Article history:
Received 12 May 2020
Received in revised form 20 October 2020
Accepted 7 November 2020
Available online xxxx

Keywords:
Seismic-while-drilling
Smart drilling
Optimal well placement
Complex reservoir
Oil sands

ABSTRACT

The oil and gas industry continuously struggles to cope with the high cost of production in the context of competitive worldwide market prices. Low oil and gas prices backstop an economic situation where exploration and exploitation of complex reservoirs are hindered. Exploration and production of complex reservoirs face several challenges. Despite having subsurface information from geological models and seismic images, they are prone to uncertainties, and as a consequence, the development and production of such reservoirs are not optimal. Here, we focus on advanced sensing methodologies that are tailored to complex unconventional reservoirs, such as the heavy oil reservoirs in Canada. Further refinement of reservoir extent, hosted oil, and geological properties can potentially increase production rate, decrease the costs and risks of drilling, alleviate well placement issues, and improve the management and monitoring of reservoir — overall leading to lower uncertainty on developing the resource. We introduce new workflows for smart drilling and optimal well placement by taking advantage of the seismic-while-drilling imaging approach. The proposed framework provides high-resolution images of the subsurface thanks to new advancements in seismic remote sensing, signal processing, and imaging.

1. Introduction

According to the statistics reported by EIA's International Energy Outlook 2017, world energy consumption is expected to increase by 15.3% over the next twenty years (EIA, 2017). However, the oil and gas industry faces a long-term downturn with oil and gas price reduction (dropped ≈ 44% from 2014 to 2017) and uncertainties. The financial weakness of operators under low oil and gas prices hinders the exploration and production of complex reservoirs such as the ones encountered in deepwater reservoirs in the Gulf of Mexico or tight heavy oil reservoirs in Canada and Venezuela. For example, difficulties of tight and heavy oil exploration and production have been extensively studied (Butler and Stephens, 1981; Heim et al., 1984; Wehunt et al., 2003; Guo et al., 2016; Montgomery and O'Sullivan, 2017; Dong et al., 2019). Moreover, the demand to reduce environmental impacts of oil and gas production is also important (Dorian et al., 2006). In this paper, we describe a new workflow to optimize drilling, well-placement, geosteering, and production of complex petroleum reservoirs, which ultimately reduces drilling costs by providing a better subsurface model.

Exploration and exploitation of complex reservoirs face several challenges. These include uncertainties in geological and geophysical models, risks and cost of drilling, and challenges in geosteering and optimal well-placement. Uncertainties inherent in the geological model of the region of interest and subsurface seismic images, provided by processing surface seismic data, should be minimized to increase the performance of drilling, well-placement, geosteering, and production. There have been many new ways to sense and monitor to better capture the structures around wells, locate high pore pressure zones, sweet spots, and barriers, and monitor dynamics of fluid movements in the reservoir during production (Ramakrishnan and Thambynayagam, 1999; Maxwell et al., 2010; Mateeva et al., 2014).

In a complex reservoir, seismic depth images may not provide an accurate structure of the reservoir especially for deeper parts of the domain Gray et al. (2001). Accordingly, sensing and monitoring the reservoir is necessary. Additional sensing and monitoring information is required along with seismic images of the subsurface to reduce uncertainties of the reservoir description (Lines et al., 1988). Multi-offset vertical seismic profiling (MVSP) can provide such information about the structure of the subsurface around the wells (Hardage et al., 1985). MVSP is rich in information and is extensively used for imaging around the wells. MVSP can image below and above the observation point

* Corresponding author.
E-mail address: nasser.kazeminojadeh@ucalgary.ca (N. Kazemi).

https://doi.org/10.1016/j.egyr.2020.11.036

in the borehole. Moreover, it has shorter raypaths and can provide higher resolution images than surface seismic (Poletto and Miranda, 2004). However, MVSP has several shortcomings. The main issues with MVSP are (1) its acquisition cost is high, (2) to acquire the data drilling must be interrupted which increases the rig time, and (3) to acquire the data, depending on the maximum offset, the drill string should be taken out of the well for one or more days without control of the well pressure which can result in a collapse of the well (Poletto and Miranda, 2004). Logging-while-drilling (LWD) is another way to gather information from around the wells (Godbey, 1967; Tang et al., 2002). LWD provides high-resolution information about the rock properties around the well within a couple of meters. Ironically, in complex reservoirs where the LWD approach can be a vital source of information about the rock properties, logging-while-drilling is not possible (Poletto and Miranda, 2004). This is because in complex areas the drilling process is not stable and it cannot be continued for a couple of meters without casing. Seismic-while-drilling (SWD) is another sensing mechanism that helps geophysicists image the structure of the subsurface layers around the wells (Rector and Marion, 1991; Poletto and Miranda, 2004). This method sometimes referred to as drillbit VSP or reserve VSP, is of great interest in subsurface imaging, drilling, well-placement, and geosteering applications (Poletto and Miranda, 2004). The necessity of developing an efficient sensing system that does not interrupt the drilling process and provides high-quality images around the wells is the main motivation behind the technique. Since the 1960s, several workflows and sensing mechanisms are proposed and used in the industry (Meehan et al., 1998; Poletto and Miranda, 2004; Anchliya, 2006). SWD has also drawn significant interest in recent years due to increased computational power in the field and improvements in the sensing devices (Meehan et al., 1993; Greenberg, 2008; Rossi et al., 2001; Vasconcelos and Snieder, 2008; Kazemi et al., 2018b). Thanks to new advances in signal processing, high-resolution SWD images of the subsurface is possible. Also, this information is used to improve the performances of drilling and well-placement in challenging reservoirs.

Another concern when dealing with complex reservoirs is the stable and efficient drilling process. Clear understanding and modeling of drill string dynamics and drillbit–rock interaction, appears to be crucial in controlling the drill string vibrations, improving the rate of penetration (ROP) of the drilling system, preventing damages to the system, and finally reducing the safety risks of the drilling operation. Moreover, the cost of drilling is at large dependent on the rig time. Accordingly, it is necessary to reduce non-productive time by increasing the rate of penetration. To do so, knowledge of the bit–rock interaction (and consequently of the underlying formation) is an important factor. Different models of friction due to the contact between the cutting device and drilling surface have been proposed in the literature (Saldivar et al., 2016). These models usually depend on the nature of the drilled rock, such a dependence of the drill string dynamic response on bit–rock interaction and formation properties is studied by Shor et al. (2015). Estimating the characteristics of the formation is not an easy task as downhole sensors are expensive and may raise potential technical risks.

To provide a reliable characterization of the formation (and consequently of the drillbit–rock interaction), SWD could appear of great interest and be the next step towards a formation-aware drilling system. SWD uses the elastic energy radiated by a working bit to determine time-to-depth and look-ahead information while drilling (Anchliya, 2006; Meehan et al., 1998). The radiated energy is recorded at the surface using an accelerometer and conventional seismic sensors (e.g., geophones or hydrophones). The SWD measurements can be used to characterize the formation ahead of the drillbit. In turn, the formation-aware drilling system provides an opportunity to update the drilling parameters in near real-time so that the system experiences a smooth rate of penetration. It also helps to be aware of hazardous areas before drilling.

Another issue is defining the optimal well path when there are uncertainties in the subsurface models. In well placement, the objective is to place the well to obtain optimal performance during production. Ideally, the locations are optimized by using a reservoir simulator with a geological model of the reservoir. However, this process is often imperfect due to time constraints and uncertainties of the inputs of the geological and reservoir simulation models. In some approaches, parameters associated with the producible hydrocarbon, such as contacted reservoir quality, is used as a fast and reliable decision proxy. Application of LWD and measurement-while-drilling (MWD) can improve real-time geosteering by providing petrophysical information, drilling measurements, and distances to boundaries while drilling (Allen et al., 1989). Reactive geosteering uses LWD measurements while the well is drilled into a given rock. The MWD system provides downhole measurements near the bit while drilling is in progress. It provides accurate and reliable information on the formation being drilled and the behavior of the drill string. The frequent data obtained from the sampling of downhole measurements in which the data is collected downhole and telemetered and detected at the surface through either the drilling fluid, electrical conductors, or the drill pipe, are implemented for better control of drilling operations (Arps and Arps, 1964; Gearhart et al., 1981). MWD systems provide essentially real-time information generally placed in two categories: (1) drilling variables and hole information, and (2) formation characteristics. Drilling variables and hole information might include hole direction and inclination, tool-face angle, weight on bit and torque, downhole temperature and pressure, mud properties, bit vibration and acceleration, and others. Formation characteristics include radioactivity (Gamma-ray), resistivity, annular temperature, and others.

SWD method records the seismic energy generated by drillbit–rock interaction, processes the data, and provides high-resolution images of the subsurface which allows for steering the well not only on logging data but also on the improved subsurface images. Formation boundaries and main geological uncertainties are identified above, below, and in front of the drill bit. This enhanced subsurface image reduces the uncertainties and provides valuable geological information for placing the well in complex reservoirs. It also provides sufficient time for decision making and drilling optimization through mapping reservoir structures and problematic zones ahead of the drill bit.

The paper is organized as follows: First, we introduce a new SWD-based imaging workflow. Then, we integrate SWD with drilling and develop a formation-aware drilling system. Finally, the issues of well placement and the importance of advanced sensing techniques in horizontal drilling are discussed. Each section has its concluding remarks. We also provide a discussion section, in the end, covering final remarks and conclusions.

2. Seismic-while-drilling imaging

This section covers the basics of our SWD imaging algorithm. Detailed and comprehensive formulation and analysis of this topic are outside of the scope of this writeup. Interested readers are referred to Kazemi and Sacchi (2014), Kazemi et al. (2018a,b) for more details.

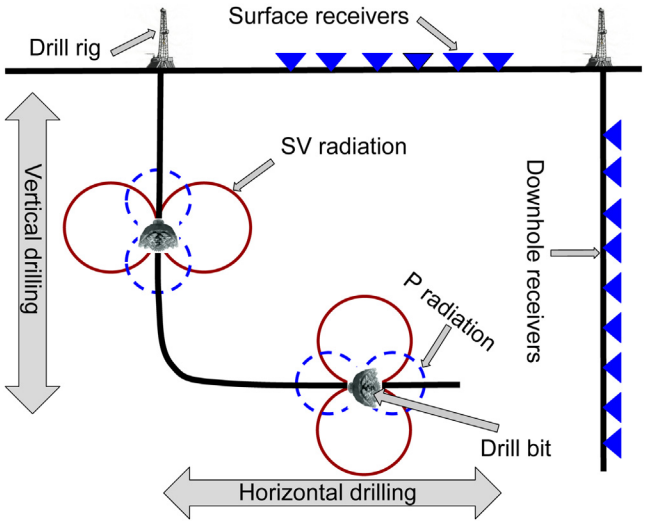

Fig. 1. Schematic representation of the geometry of receivers and drillbit sources in vertical and horizontal drilling and the radiation patterns of drillbits.

2.1. Background and motivations

The drillbit generates significant elastic wave energy whose raypaths are unique relative to those induced by standard surface seismic. Therefore, if the challenges associated with characterizing the source radiation properties can be adequately addressed, the data arising from SWD are complementary to surface data and have the potential to enhance geophysical evaluation of the subsurface. What the addition of SWD (and its raypaths) to seismic characterization provides is an opportunity to address seismic illumination issues with new measurements. In general, there are two main acquisition geometries for the SWD method. The receivers can be deployed on the surface or in the nearby boreholes, and the drillbit can be associated with vertical wells or horizontal wells. Depending on the type of drilling wells, i.e., vertical or horizontal drilling, the radiation patterns would be different. In vertical drilling, the drillbit radiation patterns in the vertical direction are dominated by the pressure component, i.e., P waves, and in the horizontal direction is mainly shear component, i.e., S waves. Hence, receivers at the surface can record the pressure wave field and provide information-rich SWD data. However, in horizontal drilling the drillbit radiation patterns in the vertical direction are dominated by the shear component, i.e., S waves, and in the horizontal direction is mainly pressure component, i.e., P waves. Accordingly, in a horizontal drilling system receivers at the surface do not record strong pressure components. Moreover, in deep and ultra-deep drilling shear wave field is highly attenuated by the earth and the quality of SWD data is poor. An alternative would be to deploy receivers in the surrounding nearby vertical boreholes and record the P component. Moreover, in downhole recording, as the distance between the drillbit location and borehole receivers are smaller compared to surface receivers, the quality of data is better. The data also contains a broader frequency range which results in providing high-resolution subsurface images. Fig. 1 is a schematic representation of the geometry of receivers, drillbit sources in vertical and horizontal drilling, and the radiation patterns of drillbits.

In complex structures wave energy penetrates weakly into some areas and surface seismic images suffer from nonuniform illumination problems. Nonuniform illumination means that some parts of the subsurface structure will be in the shadow zone of surface seismic acquisition and those regions will not be properly imaged. To remedy this shortcoming of surface seismic imaging, the SWD method along with surface seismic data is used to mitigate the nonuniform illumination problem. The idea is to combine the migrated sections of the SWD and surface seismic datasets to achieve a better illumination. To do so, the first step is to understand the seismic characteristics of the drillbit–rock interaction. In other words, we need to estimate the drillbit–rock interaction source signature. This is done by using a multichannel sparse blind deconvolution technique called SMBD (Kazemi and Sacchi, 2014). After estimating the SWD source signature, to migrate the SWD data, we forward propagate the estimated SWD source signature through the background medium and cross-correlate it with the backward propagated volume of the recorded SWD data. Finally, we merge the migrated section of the SWD data with the surface seismic image to improve the illumination. The efficiency of the workflow is tested against a benchmark model called the Sigsbee2a model which is designed to mimic the complex reservoir of the Gulf of Mexico. This challenging and complex model is difficult to image since seismic energy tends to bend towards the high-velocity salt body and the sub-salt region is in the shadow zone of the surface seismic acquisition. Hence, imaging the sub-salt region in this model faces challenges in terms of resolution, illumination, and uncertainties.

In the next section, we start by introducing seismic depth imaging methodology and its illumination problem. Then, we argue that SWD data, when used along with surface seismic data, can improve the illumination. Later, we explain the multichannel blind deconvolution algorithm for estimating the SWD source signature. Finally, a workflow presented on merging surface and SWD imaging, and the performance of the workflow is evaluated on a challenging Sigsbee2a model.

2.2. Seismic imaging and nonuniform illumination problem

We start with the description of wave equation in a constant density acoustic and isotropic medium

$$(\omega^2\mathbf{s}^2 + \nabla^2)P = f\ \delta(\mathbf{x} - \mathbf{x}_s), \tag{1}$$

where P is pressure wavefield, $\mathbf{s}$ is slowness (reciprocal of velocity), ω is temporal frequency, f is the source signature, $\mathbf{x}_s$ is source location and ∇^2 is Laplacian operator. To start the analysis, it is assumed that the background smooth velocity (slowness) field is known. We represent the squared slowness and the scalar field in terms of perturbations and backgrounds as

$$\mathbf{s}^2 = \mathbf{s}_0^2 + \mathbf{m}, \quad \textit{and} \quad P = P_0 + \Delta P, \tag{2}$$

where $\mathbf{s}_0$ and P_0 are background slowness and wavefield, respectively. The parameter $\mathbf{m}$ is the perturbation in slowness-squared. Similarly, ΔP is the perturbation in the wavefield due to $\mathbf{m}$. Now, by using the Green's function G_0 satisfying the wave equation corresponding to the background medium

$$(\omega^2\mathbf{s}_0^2 + \nabla^2)\, G_0 = \delta(\mathbf{x} - \mathbf{x}_s), \tag{3}$$

the perturbed wavefield can be calculated via

$$\Delta P(\omega, \mathbf{x}) \approx -\sum_{\mathbf{x}'} G_0(\mathbf{x}, \omega; \mathbf{x}')\, \omega^2 \mathbf{m}(\mathbf{x}')\, P_0(\omega, \mathbf{x}'). \tag{4}$$

In general, if the explosive source is at position $\mathbf{x}_s$ and the receivers are at spatial coordinates $\mathbf{x}_r$, Eq. (4) can be written as

$$\begin{aligned} d(\omega, \mathbf{x}_r, \mathbf{x}_s) &= \Delta P(\omega, \mathbf{x}_r, \mathbf{x}_s) \\ &\approx -\sum_{\mathbf{x}'} G_0(\mathbf{x}_r, \mathbf{x}_s, \omega; \mathbf{x}')\, \omega^2 \mathbf{m}(\mathbf{x}')\, P_0(\omega, \mathbf{x}'), \end{aligned} \tag{5}$$

which is the forward modeling operator. In matrix–vector notation, we have

$$\mathbf{d} = \mathbf{L}\,\mathbf{m}, \tag{6}$$

where **d** denotes the seismic measurements represented by a vector and the vector **m** stands for the acoustic potential and **L** is the forward modeling operator. Now, by defining the adjoint of forward operator, migrating the measured data is carried by

$$\mathbf{m}_{mig}(\mathbf{x}) = -\sum_{\omega}\sum_{\mathbf{x}'_s}\sum_{\mathbf{x}'_r}(\omega^2 P_0^*(\mathbf{x},\omega;\mathbf{x}'_s)\, G_0^*(\mathbf{x}'_s,\mathbf{x}'_r,\omega;\mathbf{x}) \times d(\mathbf{x}'_r,\mathbf{x}'_s,\omega)) = \mathbf{L}^T\,\mathbf{d}, \tag{7}$$

where $\mathbf{m}_{mig}$ is the migrated image of the subsurface and $\mathbf{L}^T$ is the adjoint or migration operator.

Unfortunately, $\mathbf{m}_{mig}$ is the approximated version of **m**. This can be inferred by combining Eqs. (6) and (7)

$$\mathbf{m}_{mig} = \mathbf{L}^T\,\mathbf{d} = \mathbf{L}^T\mathbf{L}\,\mathbf{m}, \tag{8}$$

where $\mathbf{L}^T\mathbf{L} \neq \mathbf{I}$. Least squares migration aims at improving the illumination by applying the inverse of the Hessian on the migrated image. Nonetheless, in the case of least squares migration, if there is no illumination (i.e., null space of the migration operator) then there is no way that least squares can recover the information. To remedy this shortcoming, more information is added about the subsurface by including the SWD dataset into the imaging problem. In other words, we aim at solving

$$\mathbf{m}_{merged} = \mathbf{L}^T\,\mathbf{d} + \mathbf{L}_{SWD}^T\,\mathbf{d}_{SWD} = [\mathbf{L}^T \quad \mathbf{L}_{SWD}^T]\,[\mathbf{d}^T \quad \mathbf{d}_{SWD}^T]^T = \mathbf{L}_{merged}^T\,\mathbf{d}_{merged}, \tag{9}$$

and we are hoping that $\mathbf{L}_{merged}^T\,\mathbf{L}_{merged} \approx \mathbf{I}$. To build the $\mathbf{L}_{SWD}^T$ operator, the SWD source signature is required. Next section describes the SWD source signature estimation algorithm.

2.3. SWD source signature estimation

Seismic while drilling data can be modeled as

$$\mathbf{d}_j = \mathbf{W}\,\mathbf{r}_j + \mathbf{n}_j \qquad j = 1,\ldots J, \tag{10}$$

where **W** is the convolution matrix of SWD source signature, **r** is reflectivity series and **n** is the noise term. After some algebraic manipulations, it is easy to show that,

$$\mathbf{D}_p\mathbf{r}_q - \mathbf{D}_q\mathbf{r}_p = \mathbf{N}_p\mathbf{r}_q - \mathbf{N}_q\mathbf{r}_p\,, \tag{11}$$

where $\mathbf{D}_p$ and $\mathbf{D}_q$ in Eq. (11) represent the convolution matrices of channels p and q, respectively. $\mathbf{N}_p$ and $\mathbf{N}_q$ are convolution matrices of noise components. The combination of all possible equations leads to the following inhomogeneous system of equations

$$\mathbf{A}\,\mathbf{x} = \mathbf{e}, \tag{12}$$

where

$$\mathbf{A} = \begin{pmatrix} \mathbf{D}_2 & -\mathbf{D}_1 & & & & & \\ \mathbf{D}_3 & & -\mathbf{D}_1 & & & & \\ \mathbf{D}_4 & & & -\mathbf{D}_1 & & & \\ \vdots & & & & \ddots & & \\ & \mathbf{D}_3 & -\mathbf{D}_2 & & & & \\ & \mathbf{D}_4 & & -\mathbf{D}_2 & & & \\ & \vdots & & & \ddots & & \\ & & & & \mathbf{D}_J & -\mathbf{D}_{J-2} & \\ & & & & & \mathbf{D}_J & -\mathbf{D}_{J-1} \end{pmatrix} \tag{13}$$

and $\mathbf{x} = [\mathbf{r}_1, \mathbf{r}_2, \mathbf{r}_3, \ldots, \mathbf{r}_J]^T$. (14)

To find the reflectivity, SMBD minimizes the following cost function

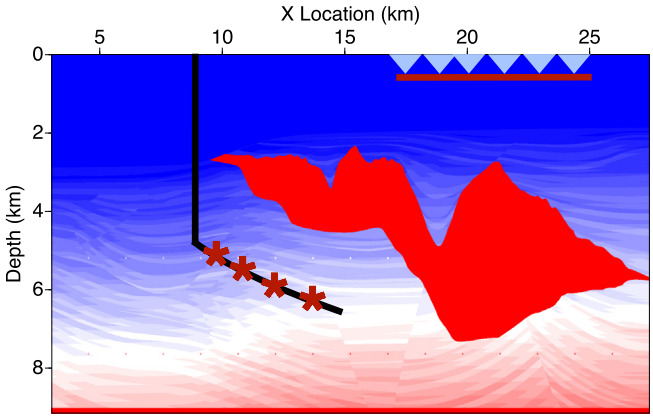

Fig. 2. Seismic-while-drilling acquisition.

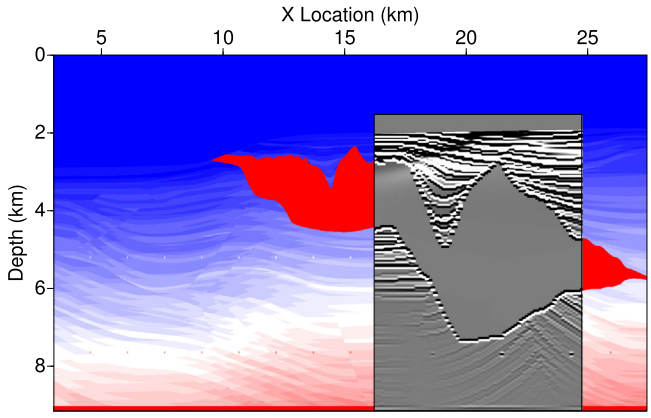

Fig. 3. Imaging result of SWD data over Sigsbee2a model.

$$\hat{\mathbf{x}} = \underset{\mathbf{x}}{\operatorname{argmin}} \quad \frac{1}{2}\|\mathbf{A}\,\mathbf{x}\|_2^2 + \lambda\sum_i(\sqrt{x_i^2+\epsilon^2}-\epsilon), \quad \text{subject to} \quad \mathbf{x}^T\mathbf{x} = 1 \tag{15}$$

where ϵ is a small number to mimic the L_1 norm behavior and λ is a regularization parameter. As a by-product, after solving for the reflectivity, SWD source signature can be estimated using the frequency-domain least squares estimator.

2.4. Numerical examples

To test the performance of the combined SWD and surface seismic imaging in improving the subsurface illumination, we simulated both surface and SWD data over the Sigsbee2a model. In the case of SWD data, we used drillbit–rock interaction as sources in the deeper part of the well and we put receivers near the surface with 9 km offset from the well's location (Fig. 2). In the case of surface seismic, sources are fired near the surface and receivers were listening to all of the shots. To generate the data, we used a second-order acoustic finite-difference modeling engine and in the case of SWD data, later we convolved the data with a drillbit source signature. To mimic the drillbit–rock signature, we assumed that every tooth of the drillbit generates a harmonic waveform (Poletto, 2005). Nonetheless, the source signature has harmonic and non-harmonic components due to the resonances between the drill string and rocks at the source locations. Moreover, to make the source signature broadband, we added a band-limited white Gaussian noise to the signature (see

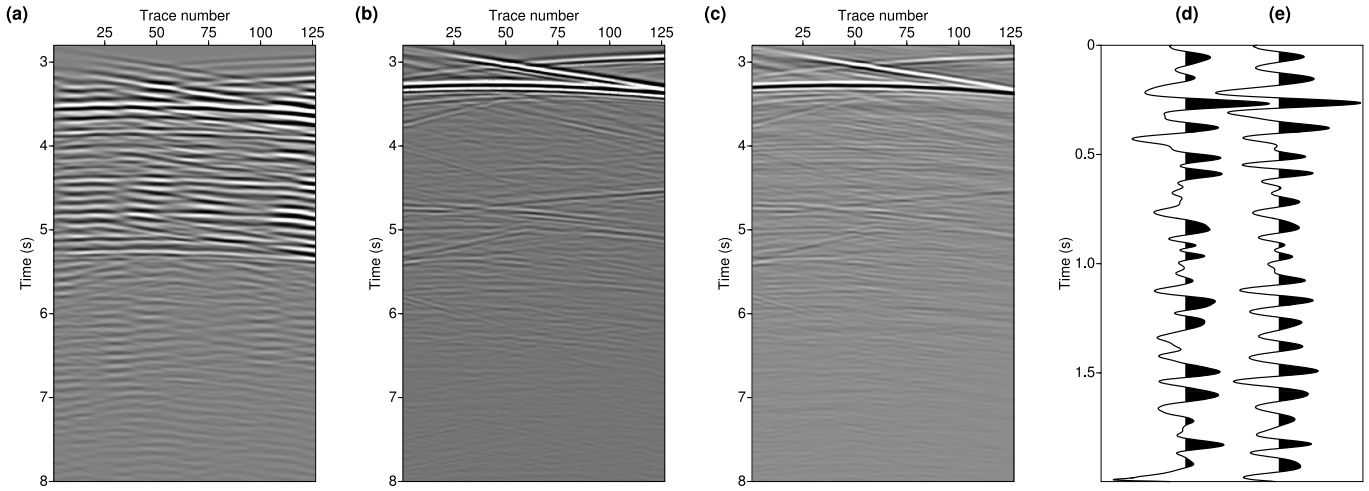

Fig. 4. Windowed version of SWD data. (a) SWD shot gather. (b) True drillbit source removed data. (c) Estimated drillbit source removed data. (d) True and (e) Estimated source signatures.

Fig. 4d). To image the SWD data, we estimated the source signature by applying the SMBD algorithm on one of the shot gathers. A windowed version of the data is depicted in Fig. 4a. True drillbit-signature-removed data and the estimated version of it are shown in Figs. 4b and c, respectively. Later, we use the estimated drillbit-signature-removed data and drillbit data to estimate the drillbit waveform. The estimated waveform is shown in Fig. 4e. Then, we feed the drillbit signature into the pre-stack reverse time migration algorithm to image the subsurface (Fig. 3). The algorithm is able to successfully image the subsurface. Comparing the SWD image with the surface seismic image, shown in Fig. 5a, we notice that under the salt region is nicely imaged by the SWD technique. On the other hand, the surface seismic image suffers from poor illumination. Finally, in Fig. 5b, by combining SWD and surface seismic data images, we can improve the subsurface image and provide a reliable and clear image of the subsurface that can be used to optimize the drilling parameters and guarantee an efficient rate of penetration. The blue square rectangle in Fig. 5b shows the common image region between the SWD and surface seismic images and arrows show the sub-salt regions where the combined image did a better job than that of the surface seismic image in improving the illumination. In the combined image, the lower boundary of the salt and the point diffractor under it are accurately imaged. Imaging and merging workflow of the surface seismic and SWD data is presented in Fig. 6.

2.5. Remarks

The drillbit generates significant elastic wave energy whose ray paths are unique relative to those induced by standard surface seismic. Provided that we understand the challenges associated with characterizing the source radiation properties of the drillbit–rock interaction, the data arising from SWD are complementary to surface data and have the potential to enhance geophysical evaluation of the subsurface. Hence, it brings an opportunity to address the seismic illumination issue by adding new measurements into the imaging problem. We used the SWD method to mitigate the illumination problem in imaging. Source signature estimation of the drillbit–rock interaction is a necessary step for pre-stack migration of the SWD dataset. To do so, we applied a multichannel sparse blind deconvolution technique to estimate the signature, and later, we fed the signature into the SWD imaging workflow. Finally, we merged the SWD image with the surface seismic migrated section to improve the illumination of the subsurface features. The efficiency of the workflow is tested against the Sigsbee2a model.

3. Formation-aware drilling system

This section reports a Formation-aware drilling system method based on the SWD measurements and drill string dynamics modeling. For a detailed explanation of the algorithm and its application for estimating the velocity of the formation while drilling and further development of the approach for improving the drill string dynamics estimation, interested readers are refereed to Kazemi et al. (2018a,b), Auriol et al. (2020b,a).

3.1. Drilling systems and challenges

The drilling of an oil well consists of creating a borehole up to several thousand meters deep into the ground until an oil reservoir is reached. If the first (onshore) wells only ran tens of meters deep, due to the evolution of the drilling techniques, deeper and thinner reservoirs can now be reached and the corresponding wells run several thousand meters deep under the seabed. The drilling rig can be located on an onshore or offshore platform, but also a drilling ship.

A drilling system mainly consists of a mechanical part and a hydraulic part. The mechanical part is made of three components: the rotating mechanism (usually a rotary table or a top drive), the drill string, and the Bottom Hole Assembly (BHA); while the hydraulic part consists of the main pump, the inner part of the drill string, the annulus and the outlet valve. Regarding the mechanical part, the rotating mechanism (located at the top of the drill string) provides the necessary torque to put the system into a rotary motion. This rotary motion, applied at the surface, is transferred to the drill string and the BHA. The drill string is mainly built from drill pipes which usually are steel tubes with a length of typically 10 m. These pipes are usually run in tension to avoid the effect of fatigue due to a potential helical buckling. They are hollow so that drilling fluid can be injected by a mud pump. This fluid has, among others, the function of cleaning, cooling and lubricating the bit, thus evacuating the rock cuttings. The BHA comprises the bit (a rock cutting device), a series of relatively heavy pipe sections, known as drill collars (much thicker pipes which provide the necessary weight to perform the perforation), stabilizers (at least two spaced apart) which prevent the drill string from unbalancing, and “shock subs” that absorb vibrations between the bit and the drill-collars. While the length of the BHA remains constant, the total length of the drill pipes may increase

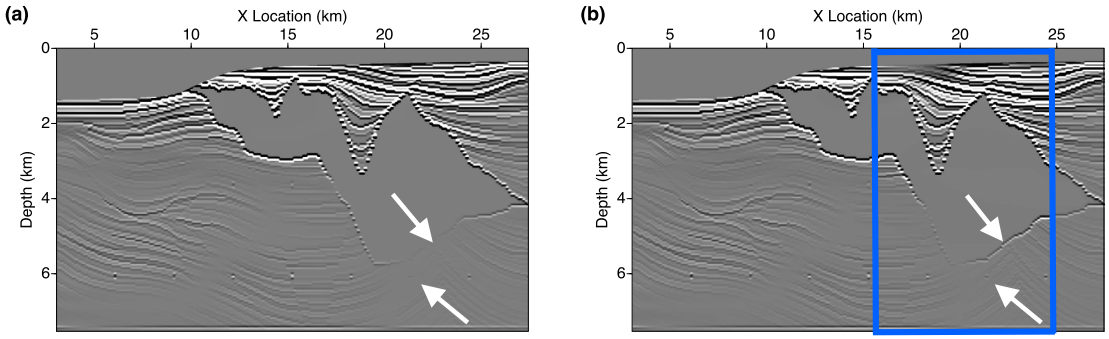

Fig. 5. Prestack RTM images of the Sigsbee2a model. (a) Surface seismic imaging. (b) Combined SWD and surface seismic imaging.

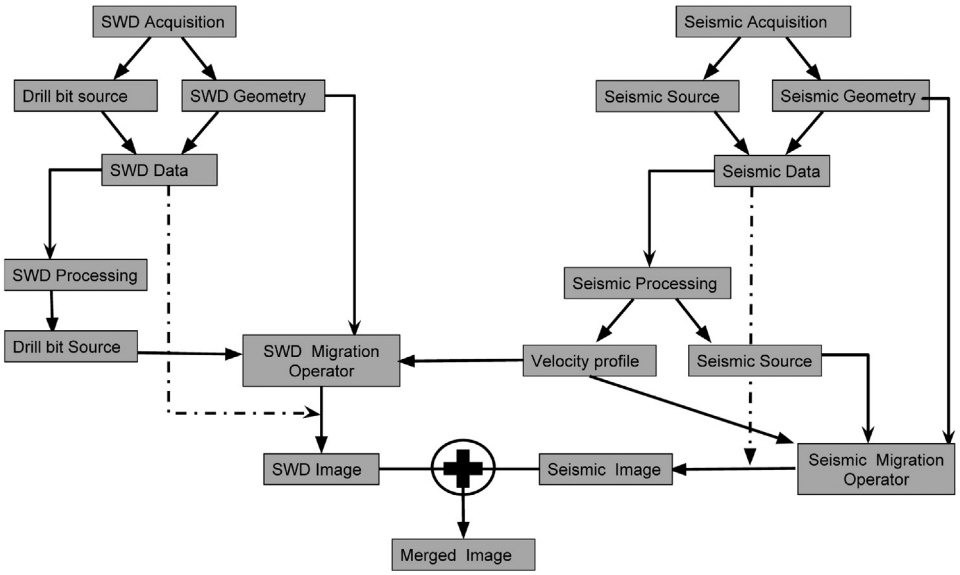

Fig. 6. Imaging and merging workflow of the surface seismic and SWD data. Note that the conditioning of datasets are necessary depending on the requirements of the migration operators.

as the borehole depth does, which explains why some pipe sections (drill pipes) are added, leaving the bit coupled at the bottom part of the set. Apart from providing the rotary motion of the drillbit, the drill string transfers necessary axial force, known as Weight On Bit (WOB), to facilitate the deep hole drilling process. Drill strings can reach lengths of several kilometers, which make them very slender structures (Kapitaniak et al., 2015). Note that to avoid the collapse of the well or damage of the formation, it is crucial to maintain the Bottom-Hole Circulating Pressure (BHCP) between pre-specified constraints.

The dynamical behavior of drill strings is complex as many dynamic phenomena are involved, such as vibrations, bending and twisting quasi-static motion, and bit–rock interactions (Kapitaniak et al., 2015; Spanos et al., 2003). Different drilling models have been proposed through the literature. The dynamics of interest (axial and torsional vibrations) can be derived by assuming elastic deformations and using equations of continuity of the state and the momentum balance. These different models can be classified into two main categories (Saldivar et al., 2016).

- **Lumped parameter models.** In this class of models, the drilling system is represented by a simple mass–spring model, abstracting the BHA inertia as a lumped mass while the drill string stiffness is represented by a torsional stiffness. Such a system can consequently be simplified in an ordinary differential equation. This finite-dimensional system representation (whose motivation relies on the need to define a simple description of drilling dynamics) provides a rough description of the dynamics taking place at different levels of the string. Although such models do not capture all the system dynamics and have a reduced accuracy, they are accurate enough to properly describe the drill string behavior and are easy enough to make the analysis simple and straightforward (Christoforou and Yigit, 2003).
- **Distributed parameter models.** In this class of models, the drill string is considered as a beam subject to axial and torsional efforts. Then, it can be modeled by a set of hyperbolic partial differential equations (namely wave equations) (Di Meglio and Aarsnes, 2015). This class of models, although much accurate compared to lumped parameter models, makes the analysis harder and may involve a higher computation cost when dealing with simulations. If the damping can be neglected, these wave equations can be reduced to neutral-type time-delay models, offering a good trade-off between the accuracy of the model and its complexity, allowing to exploit techniques from delay systems theory. Finally, one must be aware that if the dynamics of the drill string can be modeled by a set of PDEs, these equations may be different for the upper part of the drill string and the BHA as they have different inertia, Young's modulus, etc.

For both classes of representations, model inputs include drill string and BHA composition, well survey data, surface equipment,

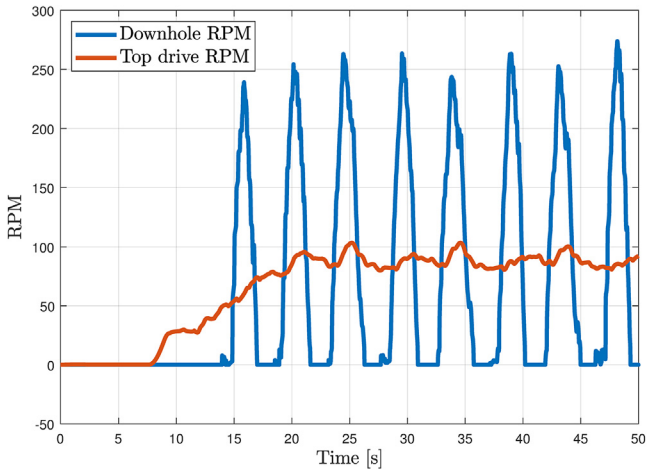

Fig. 7. Illustration of the stick–slip phenomenon by representing the top-drive and downhole velocity obtained with a simulated example.

and drilling parameters. Special attention has to be paid to the boundary conditions. More precisely, for the distributed parameter models, the wave equations describing the drilling system dynamics are uncoupled through the domain and the coupling between the axial and torsional dynamics appears through the bit–rock interaction law at the downhole boundary. Several equations describing the couplings between the torsional and axial dynamics at the boundaries of the drill string can be found in the literature (Boussaada et al., 2012; Germay et al., 2009a; Richard et al., 2004). An extensive review of drilling models and the most suitable modeling approach depending on the pursued research objective can be found in Saldivar et al. (2016).

Understanding the drill string vibrations is a crucial step as these vibrations can cause instability in the system. The drill string interaction with the borehole gives rise to a wide variety of non-desired oscillations (Dunayevsky and Abbassian, 1998; Jansen, 1993; Saldivar et al., 2011) which can be classified depending on the direction they appear

- **Longitudinal or axial vibrations.** They are produced in a vertical direction, causing a bit-bouncing effect that is rebounds of the bit at the bottom of the oil well.
- **Lateral vibrations.** These vibrations are produced when the drill string's mass center is displaced from the rotation axis. They cause a whirling phenomenon, which is whirl-like movements and rebounds within the oil well walls.
- **Torsional vibrations.** These vibrations can appear due to downhole conditions, such as significant drag, tight, hole or formation characteristics (even though as explained below, these are not the only causes). They are known as stick–slip and are considered to be one of the most prevalent vibrations. These stick–slip oscillations are characterized by a series of stopping – "sticking" – and releasing – "slipping" – events of the bit. More precisely, under certain conditions, the system enters a limit cycle. In other words, it oscillates between a stick phase, in which the velocity of the bit is equal to zero (there is an accumulation of energy) and a slip phase that consists of a sudden release of the bit that starts rotating at very high velocities (around twice the velocity of the rotary table). These oscillations are pictured in Fig. 7.

All these vibrations may lead to a reduction of the Rate of Penetration (ROP) as they deteriorate the performance of the process, cause fatigue on the equipment and wellbore instability. These vibrations can also lead to premature failure of the bit. Thus, they may cause catastrophic failures or at least wear the expensive components of the drill string (Kriesels et al., 1999). Among these different types of vibrations, numerous contributions have focused on the stick–slip phenomenon (Navarro-Lopez and Cort, 2007; Sagert et al., 2013; Bekiaris-Liberis and Krstic, 2014; Di Meglio and Aarsnes, 2015) as the torsional vibrations are considered to be the most prevalent. As mentioned above, such oscillations can be the consequence of specific downhole conditions (rock composition or small diameter of the borehole), and therefore, numerous models assume that stick–slip is a consequence of the non-linear frictional force actuating at the bit by contact with the rock formation (Leine et al., 2002; Nandakumar and Wiercigroch, 2013). More precisely, in these models, the stick–slip phenomenon is considered to be related to the velocity-weakening effect (Stribeck-like effect) of the frictional force at the bit and is insofar associated to typical dry friction profiles (static friction and dynamic friction) (Brett, 1992; Kapitaniak et al., 2015). However, one must be aware that the bit–rock interaction is not the only cause of stick–slip. Otherwise, this would not explain the occurrence of such stick–slip oscillations in the case of the off-bottom bit. This off-bottom stick–slip phenomenon is well known from the field, and is often assumed to be caused by a negative difference between static and kinematic *along-string* Coulomb-type friction (Brett et al., 1989; Halsey et al., 1986; Zhao et al., 2016). It emphasizes the action of non-linear forces along the drill string (which are combined with the bit rock interaction) in the torsional oscillatory behavior of drilling systems (Aarsnes and Shor, 2018). This is of particular importance in modern wellbores which are rarely straight and must follow preplanned well plans, ranging from simpler horizontal or deviated wells to complex three-dimensional paths, thus increasing the effect of torque and drag.

3.2. Methodology for a formation-aware drilling system

During the drilling process, the operator wants to control the downhole behavior of the drill string (e.g. reach a given rpm, a given orientation, etc.) and optimize the ROP, while avoiding undesired oscillations. To do so, it is usually possible to impose (using the rotary table) the weight on the drill string and the torque at the surface. Automated control laws have been designed to solve such control problems (Serrarens et al., 1998). Recent control laws (which are not simple PID controllers) are usually based on the previously mentioned lumped or distributed parameter models. The accuracy of these models (and therefore the performance of the associated control laws) depends on the knowledge of the drilled rock, as the downhole boundary condition depends on the bit–rock interaction. Thus, developing a formation-aware system that estimates in real-time the nature of the formation may be of prime interest as it would provide precious information about this bit–rock interaction. This knowledge of the drilled rock nature can then be used to reinforce or adjust in real-time the model (and in particular the downhole boundary condition) on which the control law is designed. This section gives some insights about a novel approach for the characterization of the formation using SWD sensing methodology. The proposed approach could lead to a formation-aware drilling system. More precisely, we propose in a simplified framework (vertical weight without any angular rotation and in the absence of damping) an algorithm that estimates the compressional and shear velocities of the formation ahead of a roller-cone drill-bit. This algorithm uses the amplitude variations of the first arrivals of the P and S-waves, in the processed seismic-while-drilling records at the surface, combined with topside hook speed and hook load measurements.

Let us consider a vertical well with a roller-cone drillbit. A distributed model proposed in Di Meglio and Aarsnes (2015), Germay et al. (2009b) is used to describe the evolution of the axial displacement $\xi(t,x)$ of the drill string. Let us denote A the cross-sectional area of the drill string and E as Young's modulus. To simplify the model, it is assumed that these parameters are constant along the drill string, they are known, and depend on the nature of the drill string (usually steel). Let us also denote t the temporal variable (which is positive) and x the spatial variable that belongs to $[0, L]$ (with L being the total length of the drilling system). The point $x = 0$ corresponds to the surface and $x = L$ corresponds to the drill-bit. The axial motion satisfies the following wave PDE

$$\frac{\partial^2\xi}{\partial t^2}(t,x) - c_\xi^2\frac{\partial^2\xi}{\partial x^2}(t,\xi) = -k_a\frac{\partial\xi}{\partial t}(t,x), \tag{16}$$

where $c_\xi = \sqrt{\frac{E}{\rho}}$, ρ being the pipe mass density, and k_a is a damping coefficient representing the viscous shear stresses acting on the pipe. A similar wave equation could be obtained for the angular displacement if there was an angular motion. The axial force can be found from the strain, given as the local relative compression: $w(t,x) = AE(\xi(t,x) - \xi(t,x+dx))/dx$, $dx \to 0$ being the infinitesimal axial position increment. The velocity can be expressed as $v(t,x) = \frac{\partial\xi(t,x)}{\partial t}$. It can be shown that the axial motion is described by the following set of PDEs

$$\frac{\partial w(t,x)}{\partial t} + AE\frac{\partial v(t,x)}{\partial x} = 0, \tag{17}$$

$$\frac{\partial v(t,x)}{\partial t} + \frac{1}{A\rho}\frac{\partial w(t,x)}{\partial x} = -k_a v(t,x). \tag{18}$$

At the topside boundary, we assume that the weight on the drill string is imposed by the operator, which yields

$$-EA\frac{\partial\xi(t,x)}{\partial x} = w_0(t).$$

To derive the downhole boundary condition, one can use a force balance on the lumped BHA. As the BHA is made of different pipes from those of the drill string (with different inertia, Young's modulus, etc.), a new set of wave PDEs for the BHA are required. However, as the length of the BHA is much smaller than the one of the drill string, its effect can be lumped into an ODE coupled with the drill string (Di Meglio and Aarsnes, 2015). As mentioned above, different expressions can be found in the literature to express this boundary condition. However, they usually use the *intrinsic specific energy* of the rock that depends on the formation. A simplified (but still accurate) expression of this bottom-hole boundary condition is given by

$$M_b\frac{\partial^2\xi}{\partial t^2}(t,L) = -\frac{a\zeta\epsilon}{\omega_{\text{bit}}}\frac{\partial\xi(t,L)}{\partial t} - w_f - EA\frac{\partial\xi(t,L)}{\partial x}, \tag{19}$$

where M_b is the mass of the lumped BHA, ω_{bit} the bit angular velocity (assumed constant here), w_f the friction weight, a the bit radius, ζ a number characterizing the inclination the cutting angle and ϵ the *intrinsic specific energy* of the rock.

Due to the complexity of this boundary condition, controlling the weight on the drill string to achieve optimal drilling performance is not an easy task. This weight on the bit has to be updated in real-time to adapt to the changing operating conditions (different types of rocks for instance). To do so, classical control procedures rely on topside drilling data and either assume the nature of the drilled rock is known or use simple PID controllers. This explains why the knowledge of the nature of the formation could lead to an improvement in the performance of the control mechanism and thus optimize ROP while drilling.

The *intrinsic specific energy* of rock is related to its compressional and shear velocities. While drilling, the drill-bit rock interaction radiates significant elastic, P- and S-wave, energy. In isotropic and homogeneous media, these radiations are functions of the drill-bit point force and the seismic velocities of rocks. It has been shown in Rector and Hardage (1992), that for a roller-cone drill bit, the seismic radiation pattern proceeding from the axial component drill-bit impacts can be modeled as a transient, monopolar point force acting along the axis of the borehole. Let us denote U_r the P-wave radiation and U_ϕ the S-wave radiation. These radiations can be measured at the surface using the SWD method described above. More precisely, the far-field radial displacement resulting from a point force, $w(t,L)$ satisfies the following relation

$$U_r(r,\phi,t) = \frac{A_1\cos(\phi)}{\rho_f\alpha^2 r}w(t-\frac{r}{\alpha},L), \tag{20}$$

and the far-field angular displacement satisfies

$$U_\phi(r,\phi,t) = \frac{A_1\sin(\phi)}{\rho_f\beta^2 r}w(t-\frac{r}{\beta},L), \tag{21}$$

where r is the straight line distance from the source to the wavefront, ρ_f is the formation density, α is the formation compressional velocity, β the formation shear velocity, A_1 is a constant, and the angle ϕ is measured relative to the direction of the point force (i.e. relative to the direction of axial drill-tooth impacts at the bottom of the borehole). Note that ρ_f can be expressed as functions of α (e.g. $\rho_f = 1.74\alpha^{0.25}$, see Brocher (2005) for details). Expressions (20)–(21) provide a relation between seismic waves and the force exerted at the bit. Each of them involves an unknown parameter (α and β) that depends on the formation. However, if the functions U_r, U_ϕ and $w(\cdot,L)$ are known, simple optimization techniques can be used to give an estimation of these parameters. The seismic time series U_r and U_ϕ can be measured using surface seismic sensors, but this is not the case for the force on the bit $w(\cdot,L)$. Nevertheless, as w is the solution of a wave equation, the function $w(\cdot,L)$ can be expressed as a (delayed) function of drill string topside hook speed and hook load, which are usually measured. For a simplified case, in which the damping term (k_a) is neglected (if this is not the case, the proof is much more technical and out of the scope of this contribution). Denoting the Riemann invariants $u(t,x) = \frac{\partial}{\partial t}\xi(t,x) - c_\xi\frac{\partial}{\partial x}\xi(t,x)$ and $z(t,x) = \frac{\partial}{\partial t}\xi(t,x) + c_\xi\frac{\partial}{\partial x}\xi(t,x)$, we immediately have using (16)

$$\frac{\partial}{\partial t}u(t,x) + c_\xi\frac{\partial}{\partial x}u(t,x) = \frac{\partial}{\partial t}z(t,x) - c_\xi\frac{\partial}{\partial x}z(t,x) = 0.$$

As u and z satisfy transport equations, we can write

$$u(t,L) = u(t-\frac{L}{c_\xi},0), \quad z(t,L) = z(t+\frac{L}{c_\xi},0).$$

Thus, we have

$$\begin{aligned}\frac{\partial}{\partial x}\xi(t,L) &= \frac{1}{2c_\xi}(z(t,L) - u(t,L))\\ &= \frac{1}{2c_\xi}(z(t+\frac{L}{c_\xi},0) - u(t-\frac{L}{c_\xi},0))\\ &= \frac{1}{2c_\xi}(\frac{\partial}{\partial t}\xi(t+\frac{L}{c_\xi},0) + c_\xi\frac{\partial}{\partial x}\xi(t+\frac{L}{c_\xi},0)\\ &\quad - \frac{\partial}{\partial t}\xi(t-\frac{L}{c_\xi},0) - c_\xi\frac{\partial}{\partial x}\xi(t-\frac{L}{c_\xi},0)).\end{aligned}$$

Using the fact that $v(t,x) = \frac{\partial}{\partial t}\xi(t,x)$ and $w(t,x) = -EA\frac{\partial}{\partial x}\xi(t,x)$, we immediately obtain

$$\begin{aligned}w(t,L) = &-\frac{EA}{2c_\xi}v(t+\frac{L}{c_\xi},0) + \frac{1}{2}w(t+\frac{L}{c_\xi},0)\\ &+ \frac{EA}{2c_\xi}v(t-\frac{L}{c_\xi},0) - \frac{1}{2}w(t-\frac{L}{c_\xi},0).\end{aligned} \tag{22}$$

Finally, using Eq. (20) and the fact that $r \geq L$ (as the well is vertical), we get

$$\frac{\partial}{\partial t}U_r(r,\phi,t) = \frac{A_1\cos(\phi)}{\rho_f \alpha^2 r} f(t - \frac{r}{\alpha}), \tag{23}$$

where f is a function obtained from (22) that only depends on $w(\cdot,0)$ and $v(\cdot,0)$ (which are measured). A similar result can be obtained for U_ϕ. Thus, using this latter expression and classical parameter estimation techniques, it becomes possible to provide in real time a reliable estimation of α (and of β using U_ϕ). Actually, from this relation, it is possible (using parameter estimation techniques) to distinguish the effect of α (that acts as a delay) and of the scaling coefficient $\frac{A_1}{\rho_f \alpha^2}$. In the general case (for which the damping term cannot be neglected), a similar relation can still be obtained, after more complex computations. It is of remarkable interest that, using the wave equation (16), we can explicitly express the state $w(t,x)$ at each point of the drill string as a function of the drill string topside hook speed and hook load, without using the downhole boundary condition.

Note that the measurements of the functions U_r and U_ϕ can be done in different locations at the surface, thus enabling an improvement of the estimated compressional and shear velocities using the redundancy of the available data.

3.3. Simulation results

This section illustrates our approach through simulation results. The drill string made of steel whose parameters are chosen as follows:

$$L = 2000 \text{ m}, \quad A = 3.5 * 10^{-3} \text{ m}^2, \quad E = 2 * 10^{11} \text{ Pa},$$
$$M_b = 12000 \text{ kg}, \quad \rho = 8000 \text{ kg m}^{-3}, \quad a = 0.1 \text{ m},$$
$$\zeta = 0.6, \quad w_f = 71280 \text{ N}, \quad \omega_{bit} = 1.05 \text{ s}^{-1}.$$

We consider three different types of formation which have different hardness (and consequently different compressional/shear velocities):

- Unconsolidated sand (i.e. water saturated) for which $\alpha = 1750$ m s^{-1}, $\rho_f = 2$ g cm^{-3} and $\epsilon = 11$ J cm^{-3}.
- Sedimentary rocks (e.g. sandstone) for which $\alpha = 3500$ m s^{-1}, $\rho_f = 2.4$ g cm^{-3} and $\epsilon = 57$ J cm^{-3}.
- Igneous or metamorphic rocks (e.g. granite) for which $\alpha = 5750$ m s^{-1}, $\rho_f = 2.7$ g cm^{-3} and $\epsilon = 151$ J cm^{-3}.

Using a Poisson ratio of 0.25, the shear velocities satisfy for each rock $\beta = \frac{\alpha}{\sqrt{3}}$. We want to estimate these velocities using the seismic measurements (20)–(21) and topside hook speed and hook load measurements. The model, which is use to simulate the drilling system, is given by (16)–(19). This section only considers an axial movement of the drill string in the absence of damping ($k_a = 0$). Even if the new methodology proposed in the previous section does not require the expression of the downhole boundary condition, this condition is necessary for simulation purposes. We have pictured in Fig. 8 the functions $U_r(r,\phi,t)$ for the three different rocks. A single seismic sensor located at the top of the well (i.e. $r = L$ and $\phi = 0$). Note that this example is only for illustration purposes as the initial condition of the drill string and the control law have been arbitrarily chosen (constant initial condition and pulse).

Expression (23) is used to estimate the formation compressional velocity α, in the case of sedimentary rocks, where $\hat{\alpha}$ denotes the estimation of α. We measure the functions $U_r(L,0,\cdot)$, $w(\cdot,0)$, and $v(\cdot,0)$, and consequently the function f defined

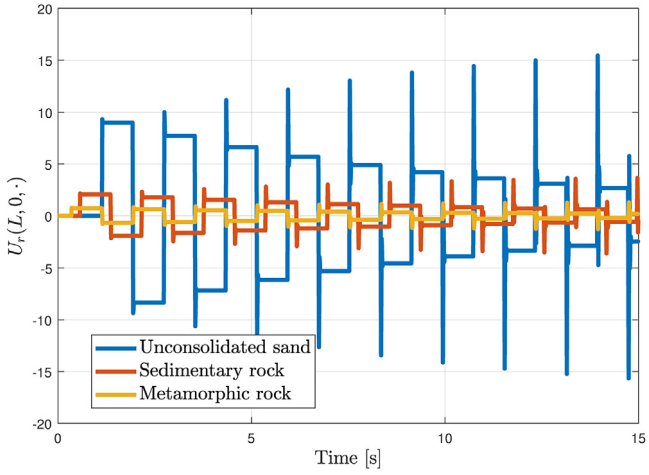

Fig. 8. Evolution of U_r (normalized) with respect to time for different rocks. The seismic sensor is located at the top of the drill string.

in (23). A set of N measurements is recorded at N different moments: $t_1, \ldots, t_N$. The goal is to find $\hat{\alpha}$ that solves the following least squares optimization problem

$$\min_{\hat{\alpha}} \quad \sum_{i=1}^{N} (U_r(L,0,t_i) - \frac{A_1}{\rho_f(\hat{\alpha})\hat{\alpha}^2 L} f(t_i - \frac{L}{\hat{\alpha}}))^2. \tag{54}$$

This optimization problem can easily be solved using classical algorithms. In the presence of white Gaussian noise in the measurements, we obtain the estimation $\hat{\alpha} = 3717$ m s^{-1}, which is close to the real value. Note that we only give here some insights for this new approach and that the proposed methodology can be easily improved:

- either by increasing the number of seismic sensors (redundancy of the information and robustness);
- or by pre-filtering the data.

Moreover, rather than using a finite number of points, one could use a sliding window to update the estimation in real time. The next steps consist in proving that (23) still holds in presence of damping (with some adjustments in the expression of f) and to test the proposed approach against real data.

3.4. Remarks

The cost of drilling a well is related to the time it takes to drill it. Thus, during drilling processes, specific attention is paid to reducing non-productive time and increasing the rate of penetration. Moreover, from a security point of view, the drill string interaction with the borehole gives rise to a wide variety of non-desired oscillations that may lead to a reduction of the ROP, but also cause fatigue on the equipment, create wellbore instability or lead to premature failure of the bit. In this context, several control techniques have been developed towards the goal of optimizing ROP and avoiding these undesired oscillations. Such techniques may be limited in the field situation due to the large uncertainty and significant complexity of the downhole dynamics of the drilling system. To increase the efficiency of existing control methods (and insofar reducing cost and time of operation), drill bit seismic can be of specific interest. More precisely, measuring P and S-waves at the surface, we have shown in a simplified case that combining these seismic-while-drilling measurements with a wave equation representation of the drill string dynamics could lead to efficient and reliable estimation of

the seismic velocities of rocks ahead of the drill bit, enabling a more precise characterization of the formation. Combining the estimation stage with existing and efficient control laws could then lead to the improvement of the drilling performances. This new methodology is the first step towards a formation-aware drilling system.

4. Optimal well placement in tight oil sand reservoirs

This section reports the application of the SWD imaging algorithm for optimal well placement in tight oil sand reservoirs. To better understand the potential and challenges of using SWD imaging for optimizing the well placement and improving the production rate, interested readers are referred to Kazemi et al. (2018a,b), Nejadi et al. (2020).

4.1. Background and motivations

Not only will detailed mapping of the underlying deposits allow more predictive reservoir modeling to occur but also, in turn, it leads to a better well placement. However, depending on the area of interest, the poor vertical well spacing may still not be ideal to develop a geological or reservoir model with confidence. For example, if the vertical well spacing is limited, small mud packages that will still have an effect on reservoir development may not be captured. Because of this, horizontal wells drilled in the area may encounter unexpected hindrances even with a proper geological model according to mapping using vertical wells. SWD can be employed in such areas to guide the drillbit towards more favorable areas and to avoid low permeability layers. Moreover, drilling decisions such as identification of coring and casing points, hazardous areas and overpressured zones are enhanced with the use of SWD (Cornish et al., 2007). While traditional LWD and MWD techniques help to further the accuracy of geological models by providing petrophysical measurements along a horizontal well, these parameters can only be analyzed once the drillbit has already passed through a potentially hazardous zone. The advantage of SWD is the real-time feedback as the tool is placed directly at the drillbit, rather than slightly behind it (Esmersoy et al., 2001). This section analyzes the optimal well placement issues in terms of cost and net present value (NPV) over McMurray Formation (Carrigy, 1959). In McMurray Formation, steam-assisted gravity drainage (SAGD) approach is used to produce the viscous bitumen from oil sands. To do so, we first start with the geology model of the area. Then explain the reservoir model and its NPV for each well pad in the SAGD setting. Next, we connect the NPV values to the uncertainties in well placement and lack of high-resolution images of the subsurface. Last, we show the possibility of acquiring a high-resolution SWD image of the subsurface over a realistic model, which is representative of McMurray Formation; and argue that such an image could have had improved the horizontal well placement.

4.2. Geology of the McMurray formation

The Lower Cretaceous McMurray Formation is part of the Athabasca Oil Sands in northeastern Alberta, where primary hydrocarbon-bearing units are found within ancient fluvial deposits of the Middle McMurray Formation (Carrigy, 1959). The McMurray Formation was deposited on top of underlying Paleozoic carbonates, creating a sub-Cretaceous unconformity. Deposited of the McMurray Formation ended with a major sea level rise and deposition of the transgressive Clearwater Formation (Leckie and Smith, 1992; Flach and Mossop, 1985). Ancient channels of the McMurray Formation flow towards the north, following the main paleo-valley heading towards the Boreal Sea (Fustic, 2007; Patruyo, 2010). The Middle McMurray Formation is composed of thick (sometimes upwards of 50 m) fining-upward point bar successions. These point bar deposits often exhibit thick packages of massive to cross-stratified sandstones near their base and have interbedded sandstones and siltstones referred to as inclined heterolithic strata (IHS) near their tops (Thomas et al., 1987; Labrecque et al., 2011). These thick sands are the main target for hydrocarbon exploitation, and adjacent sand bodies can increase the reservoir volume even further. Bitumen is recovered from the McMurray Formation by either surface mining or by in-situ methods, depending on the depth of the reserve. Because eighty percent of Alberta's Oil Sands are recovered using in-situ methods, understanding the associated challenges is important. One of the main in-situ methods is steam-assisted gravity drainage (SAGD), where two horizontal wells placed 5 m apart vertically. The upper well injects steam, heating the viscous bitumen and allowing it to flow downwards to the production well (Butler and Stephens, 1981; Strobl et al., 1997). It is therefore vital to understand where there may be any barriers to both steam and bitumen flow. Heterogeneities within the reservoir zone can hinder the development of the resulting steam chamber (Zhang et al., 2007; Chen et al., 2008; Gates et al., 2008; Gotawala and Gates, 2010; Peacock, 2010) and production performance is shown to be heavily affected by these internal heterogeneities (Su et al., 2013, 2014). Fluvial processes related to meander-belt evolution such as point bar formation, intra-point bar erosion, counter-point bar formation, and channel abandonment contribute to major heterogeneities within these deposits that have a major impact on reservoir connectivity (Jackson, 1976; Thomas et al., 1987; Smith et al., 2009; Willis and Tang, 2010; Hubbard et al., 2011; Durkin et al., 2015). The youngest, best-preserved meander-belts of the McMurray Formation have been extensively studied using 3D seismic data, well logs and core and heterogeneities within reservoirs in this interval can be estimated with some confidence (Hubbard et al., 2011; Su et al., 2013, 2014; Durkin et al., 2017). Often horizontal SAGD well pairs are placed below the well-characterized youngest meander deposit, so it is also important to have an understanding of the underlying units. However, the older deposits are often overlooked due to the lack of lithologic contrast and resolution of seismic data at these depths. Geological models that incorporate the underlying units often do not consider the geology at the same level of detail as meander-belts that are imaged with seismic. For example, Su et al. (2013, 2014) refer to the underlying units as remnant channel successions, with no emphasis on the specific architecture. To begin to understand the distribution of channel elements in the underlying deposits without the use of seismic data, core descriptions and stratigraphic dip analysis are used (Fustic, 2007). Incision by the overlying meander-belt makes correlations difficult and adds to the complexity of reservoir characterization when vertically stacked meander-belts are considered.

4.3. Reservoir model of McMurray formation

A detailed geological model and the corresponding reservoir models of the well pads are constructed from the Surmont Phase 1 SAGD project located approximately 70 km southeast of the city of Fort McMurray, AB, Canada. The formation under development is the Cretaceous McMurray. A typical vertical profile of the McMurray Formation in the area used for this study shows an overall fining upward sequence composed of a series of upward fining cycles. It consists of a meander-belt deposit in the uppermost part of the McMurray Formation and underlying older deposits. Thin, regionally deposited fine-grained sandstone and mudstone cover the meander-belt deposit in the study area. The top of the reservoir (cap rock) is defined by a marine flooding surface at the base

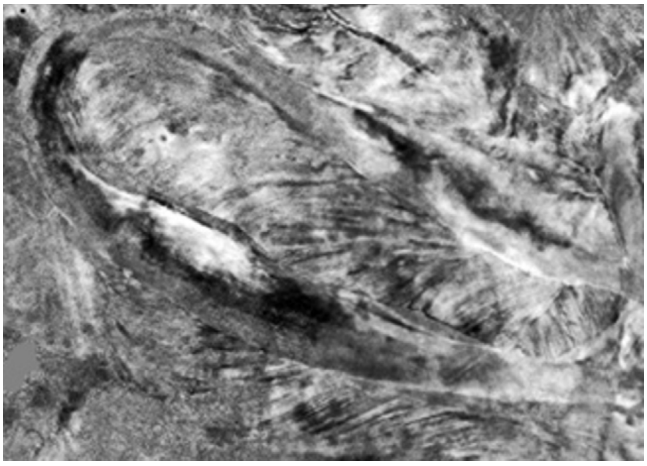

Fig. 9. Seismic depth slice of the area under study showing the abandoned channel fill and associated depositional elements of the point bar.
Source: Adapted from Durkin et al. (2017).

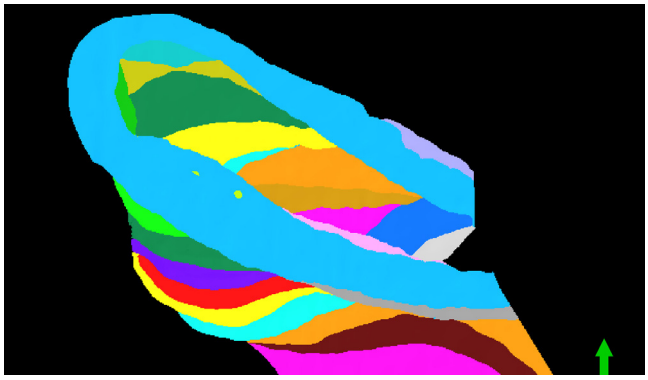

Fig. 10. Zone model of the reservoir under study for the uppermost part of the McMurray Formation.
Source: Adapted from Durkin et al. (2017).

Table 1
Reservoir parameters and constraints for the Surmont Phase 1 SAGD project.

Reservoir properties	Values
Reservoir Depth	400 m
Average Porosity	35%
Average Horizontal Permeability	3500 mD
Average Vertical Permeability	2100 mD
Average Oil Saturation (Reservoir Facies)	80%
Initial Reservoir Temperature	7°
Circulation period	80 days
Relative Permeability End Points – Reservoir Facies	
Oil–Water System	$S_{orw} = 0.40$, $S_{wc} = 0.12$
Oil–Gas System	$S_{gc} = 0.05$, $S_{org} = 0.40$

of the Wabiskaw Member. To enhance the predictive capabilities of the modeling, detailed geological features of the meandering channel belt deposits are considered in the model construction. The geological model not only reflects the complex rock properties in three-dimensional (3D) space but also includes spatial distribution characteristics of inner structural elements. Durkin et al. (2017) have used 3D seismic data of the uppermost part of the McMurray Formation and identified depositional elements comprising the fill of channel bodies. Fig. 9 shows the seismic depth slice of the area. Meander-belt and point bars can be tracked in this seismic section. The depositional elements in Durkin et al. model include point bars, counter point bars, side bars, and abandoned channel fills (Fig. 10). Each depositional element is constructed as a separate zone in the model, which captures the 3D representation of the geobody. Then, each zone internally layered based on bedding characteristics (e.g., dipping lateral-accretion surfaces in point-bar deposits). Five main lithofacies, i.e., Sandstone, Siltstone-clast Breccia, Sandstone-dominated IHS, Siltstone-dominated IHS, and Siltstone, comprise the depositional elements in the study region as described in Durkin et al. (2017), Hubbard et al. (2011). Facies distributions (histogram) are constrained to the depositional elements and the proportions are derived from petrophysical interpretations at the well locations. For instance, in the Abandoned Channel, the dominant facies is Siltstone and the proportions of other facies are negligible, whereas, in a Point-Bar, all rock types are present. In modeling facies, local facies observations (conditioning hard data at the well locations), as well as facies variability from secondary trend information, are considered in geological modeling. Table 1 summarizes the reservoir parameters and constraints of the model.

4.4. Well placement and production issues in McMurray formation

Drilling operations through complex fluvial meander-belt deposits can be extremely challenging. The geological models are often limited to the resolution of the seismic data and the sampling from drilled wells is poor. To optimize production performance and maximize NPV from SAGD reservoirs, optimal horizontal oil producer and steam injection well placement requires advanced geosteering. Well planning and the location of horizontal sections of SAGD well pairs within the reservoir is a challenge to field development. The notion of optimal well placement in SAGD is (1) drilling in the most favorable and productive reservoir rock (highest permeability), (2) placing the producer near the base of the reservoir (approximately 2 meters above the base) to maximize draining the liquids, (3) maintain sufficient distance with the base rock and possible underlying high water saturation zones, (4) avoid drilling into non-reservoir rocks (IHS, Lower early McMurray mudstones (paleosols), or abandoned channel deposits). In this work, optimal well placement is defined in terms of well pair performance that is evaluated by drilling in the most favorable reservoir rock. Fig. 11 displays the well deviation survey and gamma-ray (GR) well logs for two different well pairs in a well pad. The average vertical separation distance between the injector (upper well) and producer (lower well) are 5 m and the approximate length of the wells is 850 m (except well pair A - injector). The vertical exaggeration is 12 times. The colored curves show the Gamma Ray log along with the drilled horizontal sections of the wells. A GR cut off value of 75 API is used to differentiate reservoir and non-reservoir rock types. Low GR (red to yellow) represents reservoir facies (Sandstone, Siltstone-clast Breccia, and Sandstone-dominated IHS) and a GR greater than 75 API (cyan, light and dark blue) shows non-reservoir rocks, i.e. Siltstone-dominated IHS, and Siltstone. Generally speaking, the geological features of the reservoir and rock types in the region of the well pad are identical. However, due to poor well placement, approximately 140 meters of production well in well pair A has been drilled in low permeability non-reservoir rocks. As shown in Fig. 11 - Well Pair A, only 709 m of the total 846 m of the producer is exposed to reservoir rock and can effectively produce fluids. The horizontal section length of the corresponding injection well – Well Pair A, has been drilled according to the producible length of the production well and is 714 m, which is 136 m shorter than the pad average. The length of horizontal sections for a typical well pair design in this pad is 850 m. Table 2 summarizes the total length of the horizontals compared to the

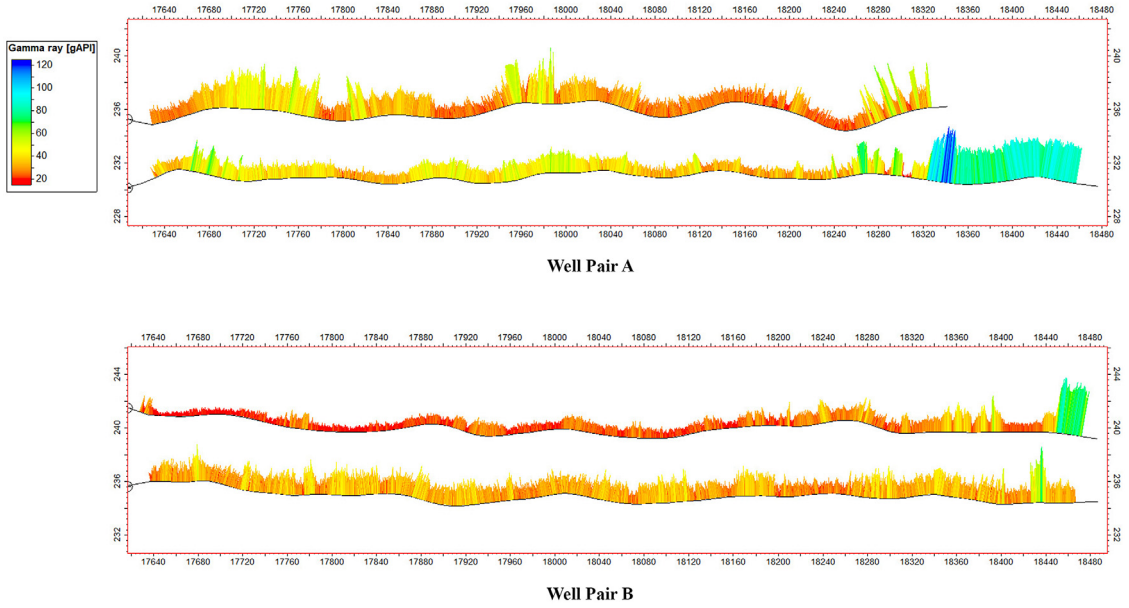

Fig. 11. Well deviation survey and gamma ray (GR) logs for two different well pairs. Well pair A has low production performance, whereas, Well pair B has a superior performance compared to the pad average.

Table 2
Total length of the horizontal sections compared to their effective lengths drilled in reservoir facies.

	Horizontal Section (m)	Reservoir Facies (%)	Actual Production length (m)
Well Pair A - Injector	714	99	714
Well Pair A - Producer	846	81	709
Well Pair B - Injector	860	97	860
Well Pair B - Producer	850	99	850
Pad average	850	97	850

effective lengths (drilled in the reservoir and permeable facies) of the wells.

The deficiencies in geosteering and drilling into low permeability rock types directly affect the production efficiency of the well pairs. The average oil production rate of the well pair A is approximately half of the pad and the cumulative steam-oil ratio (cSOR) is 3.6 m^3/m^3. The average cSOR of the pad is 3.4 m^3/m^3. Well pair B, which is one of the good pairs in this pad has a cSOR of 2.8 m^3/m^3. Table 3 presents the average normalized steam injection rate, and the normalized oil production rate of the well pairs compared to the pad average. Normalized injection and production rates are characterized by a wells injection or production rates relative to the whole pad rates.

The geosteering and well placement practices in McMurray Formation could be improved if the advanced sensing and imaging of the subsurface were implemented in the process. To provide more insight into the application and usefulness of SWD-based imaging techniques in the well placement of tight oil sand reservoirs, we generated a realistic model of subsurface geology that is representative of the complexities encountered in McMurray Formation. Fig. 12a is the 2D velocity model that shows a tight oil sand reservoir around 400 m with an average thickness of 20 m. We simulated a surface seismic acquisition over the model with sources and receivers deployed at the surface. We used 35 equally spaced shots at the surface, and the receivers were densely deployed with 2 m intervals from left to right of the mode covering the whole region. Fig. 12b shows the depth migrated image of the surface seismic data around the reservoir. As clear, seismic depth image could reveal the main structures of the subsurface, however, it struggles to provide the high-resolution image with details. The regions with uncertainties and illumination problems are marked with arrows. To further improve the resolution of subsurface images and lower the depth uncertainties, we also simulated an SWD-based acquisition geometry. The geometry of production and injection SAGD well pairs are borrowed from the real data. We simulated five SWD shot gathers by recording the pressure component of the seismic energy radiated from drillbit–rock interaction in the horizontal section of the production well. The geometry of SWD acquisition is represented in Fig. 13a. The SWD shots are equally spaced with horizontal locations varying from 1400 m to 1550 m. In horizontal drilling, pressure wavefields, i.e., P waves, are dominant in the horizontal direction, hence we deployed the receivers in downhole inside the vertical well around 3100 m. Fig. 13b shows the SWD-based image around the reservoir interval between the SWD sources and the vertical well. Rectangle regions on the SWD-based depth image show the regions where surface seismic image suffered from low resolution and had uncertainties in depth. Contrary, the SWD-based image, thanks to the unique ray paths of SWD acquisition, provided a high-resolution image of the target region. The use of SWD in the McMurray formation could reduce the issues encountered in well placement and improve the rate of production. For example, if an SWD-based image was available at the time of well placement the production well in well pair A (Fig. 11) should be stopped before drilling into the mud package.

4.5. Remarks

The issues and challenges of well placement in the presence of uncertainty in the geological model and seismic depth images are discussed. The tight heavy oil reservoirs are prone to inefficient well placement, as the surface seismic images usually do not provide accurate images of the subsurface, especially in the deeper part of the model. We used McMurray Formation to evaluate the production rate of SAGD well pairs and relate the rate of production to uncertainties in the subsurface models.

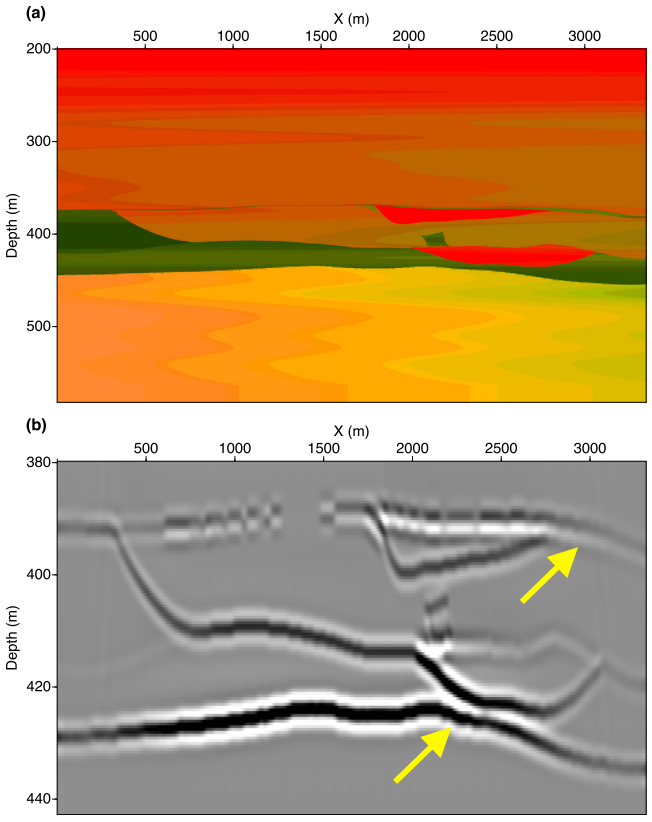

Fig. 12. Surface seismic image over a synthetic model representative of McMurray Formation. (a) Velocity model. (b) Surface seismic image. Arrows show the regions where surface seismic image has low resolution.

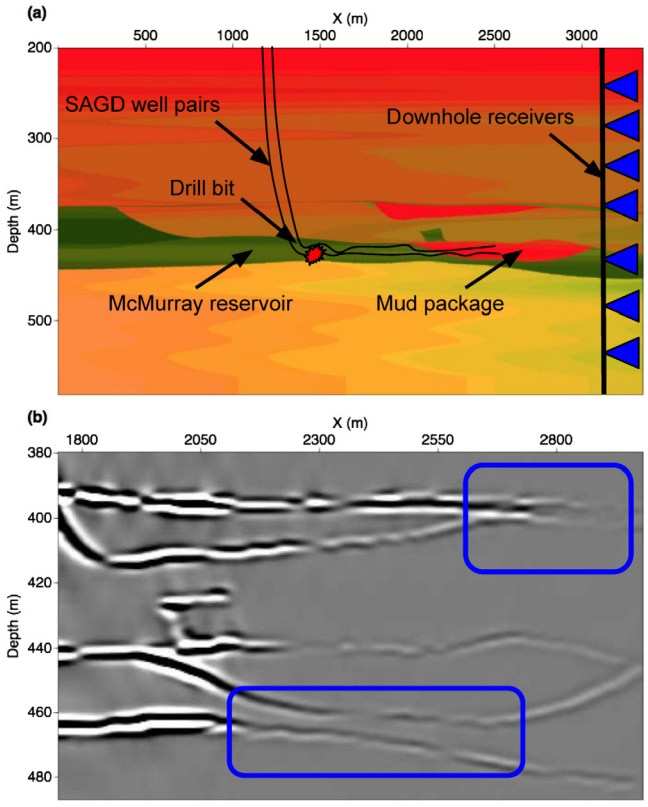

Fig. 13. Seismic-while-drilling acquisition and image over a synthetic model representative of McMurray Formation. (a) Velocity model and geometry of SAGD well pairs. Downhole receivers is used to record the drillbit seismic energy. (b) SWD image. Rectangle regions show the locations where SWD image has superior resolution compared to surface seismic image shown in Fig. 12b.

Table 3
Normalized steam injection rate, oil production rate, and cumulative steam-oil ratio of the well pairs compared to the pad average.

Well Pair	Normalized Steam Injection Rate	Normalized Oil Production Rate	cSOR $\frac{m^3}{m^3}$
A	0.59	0.51	3.6
B	1.14	1.28	2.8
Pad average	1	1	3.4

We showed that due to the lack of resolution of the models the production well in well pair A is drilled into the low permeable layer. If high-resolution images of the subsurface were available the drilling of the production well should be stopped, or the well path is updated to void drilling into the non-reservoir rocks. Using a realistic model of the McMurray Formation we showed that the SWD approach has the potential of providing such an image.

5. Conclusions

We have developed advanced sensing workflows that are tailored to complex reservoirs such as the tight heavy oil reservoirs in Canada. Our methodologies started with introducing a new SWD-based imaging algorithm. We showed that the drillbit follows ray paths that are unique relative to those induced by standard surface seismic and the data arising from SWD have the potential to enhance geophysical evaluation of the subsurface. We used the SWD method to mitigate the illumination problem in the imaging of complex reservoirs. Two realistic models that are representative of challenging Gulf of Mexico deep-water and tight oil sand reservoirs in McMurray Formation are generated. SWD image in both cases provided high-resolution images of the subsurface and improved the illumination problem inherent in surface-only seismic imaging.

Next, we introduced a smart drilling mechanism that takes advantage of SWD-based sensing. The smart drilling system combined the SWD measurements with a wave equation representation of the drill string dynamics and provided an efficient and reliable estimation of the seismic velocities of rocks ahead of the drill bit, enabling a more precise characterization of the formation. The formation characteristics can be further used to design efficient control laws for improving the drilling performances.

Finally, we discussed the well placement issues in the context of McMurray Formation. McMurray Formation is a challenging tight oil sand reservoir in Canada. We analyzed the performances of well pairs in this region, and draw interesting relationships between the uncertainties of the subsurface model and rate of production. We showed that the surface seismic images suffer from non-uniform illumination, resulting in the inefficient placing of wells. Our SWD-based images on the realistic model of McMurray Formation revealed high-resolution images of the subsurface comparing to that of the surface seismic. Accordingly, the use of the SWD image in this region could add value to the placement of the wells and provide higher production rates.

CRediT authorship contribution statement

Nasser Kazemi: Conceptualization, Methodology, Software, Validation, Formal analysis, Writing - original draft, Writing - review & editing. **Siavash Nejadi:** Conceptualization, Methodology, Software, Validation, Formal analysis, Writing - original draft.

Jean Auriol: Conceptualization, Methodology, Software, Validation, Formal analysis, Writing - original draft. **Jordan Curkan:** Formal analysis, Writing - original draft. **Roman J. Shor:** Conceptualization, Project administration, Writing - review & editing. **Kristopher A. Innanen:** Conceptualization, Writing - review & editing. **Stephen M. Hubbard:** Conceptualization, Writing - review & editing. **Ian D. Gates:** Conceptualization, Writing - review & editing, Funding acquisition.

Declaration of competing interest

The authors declare that they have no known competing financial interests or personal relationships that could have appeared to influence the work reported in this paper.

Acknowledgment

The authors would like to acknowledge the financial support from the University of Calgary's Canada First Research Excellence Fund (CFREF) program on unconventional resources.

References

Aarsnes, U.J., Shor, R.J., 2018. Torsional vibrations with bit off bottom: Modeling, characterization and field data validation. J. Petrol. Sci. Eng. 163, 712–721. http://dx.doi.org/10.1016/j.petrol.2017.11.024, URL: http://linkinghub.elsevier.com/retrieve/pii/S0920410517309075.

Allen, D., Bergt, D., Best, D., Clark, B., Falconer, I., Hache, J.-M., Kienitz, C., Lesage, M., Rasmus, J., Roulet, C., Wraight, P., 1989. Logging while drilling. Oilfield Rev. 1, 4–17.

Anchliya, A., 2006. A review of seismic while drilling (SWD) techniques: A journey from 1986 to 2005. In: SPE Europec/EAGE Annual Conference and Exhibition. Society of Petroleum Engineers, Vienna, Austria, p. 27. http://dx.doi.org/10.2118/100352-MS.

Arps, J.J., Arps, J.L., 1964. The subsurface telemetry problem-A practical solution. J. Pet. Technol. 16 (05), 487–493.

a Auriol, J., Kazemi, N., Innanen, K., Shor, R.J., 2020. Combining formation seismic velocities while drilling and a PDE-ODE observer to improve the drillstring dynamics estimation. In: 2020 American Control Conference (ACC). IEEE, pp. 3120–3125. http://dx.doi.org/10.23919/ACC45564.2020.9147966.

b Auriol, J., Kazemi, N., Shor, R.J., Innanen, K.A., Gates, I.D., 2020. A sensing and computational framework for estimating the seismic velocities of rocks interacting with the drill bit. IEEE Trans. Geosci. Remote Sens. 58 (5), 3178–3189. http://dx.doi.org/10.1109/TGRS.2019.2950257.

Bekiaris-Liberis, N., Krstic, M., 2014. Compensation of wave actuator dynamics for nonlinear systems. IEEE Trans. Automat. Control 59 (6), 1555–1570. http://dx.doi.org/10.1109/TAC.2014.2309057, URL: http://ieeexplore.ieee.org/lpdocs/epic03/wrapper.htm?arnumber=6766692.

Boussaada, I., Mounier, H., Niculescu, S.-I., Cela, A., 2012. Analysis of drilling vibrations: A time-delay system approach. In: 2012 20th Mediterranean Conference on Control & Automation (MED). IEEE, pp. 610–614.

Brett, J.F., 1992. The genesis of bit-induced torsional drillstring vibrations. SPE Dril.l Eng. 7 (03), 168–174. http://dx.doi.org/10.2118/21943-PA, URL http://www.onepetro.org/mslib/servlet/onepetropreview?id=00021943{&}soc=SPE, http://www.onepetro.org/doi/10.2118/21943-PA.

Brett, J.F., Beckett, A.D., Holt, C.A., Smith, D.L., 1989. Uses and limitations of drillstring tension and torque models for monitoring hole conditions. SPE Drill. Eng. 4 (03), 223–229. http://dx.doi.org/10.2118/16664-PA, URL: http://www.onepetro.org/doi/10.2118/16664-PA.

Brocher, T.M., 2005. Empirical relations between elastic wavespeeds and density in the earth's crust. Bull. Seismol. Soc. Am. 95 (6), 2081–2092.

Butler, R.M., Stephens, D.J., 1981. The gravity drainage of steam-heated heavy oil to parallel horizontal wells. J. Can. Pet. Technol. 20 (02), 8. http://dx.doi.org/10.2118/81-02-07.

Carrigy, M., 1959. Geology of the McMurray Formation-Part III-General Geology of the McMurray Area. Research Council of Alberta, Memoir1, 130p.

Chen, Q., Gerritsen, M.G., Kovscek, A.R., et al., 2008. Effects of reservoir heterogeneities on the steam-assisted gravity-drainage process. SPE Reserv. Eval. Eng. 11 (05), 921–932.

Christoforou, A., Yigit, A., 2003. Fully coupled vibrations of actively controlled drillstrings. J. Sound Vib. 267 (5), 1029–1045.

Cornish, B., Deady, R., Varsamis, G., Hilton, T., 2007. Multisensor seismic while drilling: Field-test results. In: SEG Technical Program Expanded Abstracts 2007. Society of Exploration Geophysicists, pp. 368–372.

Di Meglio, F., Aarsnes, U.J.F., 2015. A distributed parameter systems view of control problems in drilling. IFAC-PapersOnLine 48 (6), 272–278.

Dong, X., Liu, H., Chen, Z., Wu, K., Lu, N., Zhang, Q., 2019. Enhanced oil recovery techniques for heavy oil and oilsands reservoirs after steam injection. Appl. Energy 239, 1190–1211.

Dorian, J.P., Franssen, H.T., Simbeck, D.R., 2006. Global challenges in energy. Energy Policy 34 (15), 1984–1991.

Dunayevsky, V.A., Abbassian, F., 1998. Application of stability approach to bit dynamics. SPE Drill. Complet. 13 (2), 22–25. http://dx.doi.org/10.2118/30478-PA, https://www.onepetro.org/journal-paper/SPE-30478-PA.

Durkin, P.R., Boyd, R.L., Hubbard, S.M., Shultz, A.W., Blum, M.D., 2017. Three-dimensional reconstruction of meander-belt evolution, Cretaceous McMurray formation, Alberta Foreland Basin, Canada. J. Sediment. Res. 87 (10), 1075–1099.

Durkin, P.R., Hubbard, S.M., Boyd, R.L., Leckie, D.A., 2015. Stratigraphic expression of intra-point-bar erosion and rotation. J. Sediment. Res. 85 (10), 1238–1257.

EIA, 2017. International energy outlook. US Energy Information Administration.

Esmersoy, C., Underhill, W., Hawthorn, A., et al., 2001. Seismic measurement while drilling: Conventional borehole seismics on LWD. In: SPWLA 42nd Annual Logging Symposium. Society of Petrophysicists and Well-Log Analysts.

Flach, P.D., Mossop, G.D., 1985. Depositional environments of Lower Cretaceous McMurray Formation, Athabasca Oil Sands, Alberta. AAPG Bull. 69 (8), 1195–1207.

Fustic, M., 2007. Stratigraphic dip analysis–a novel application for detailed geological modeling of point bars, and predicting bitumen grade, mcmurray formation, muskeg river mine, northeast alberta. Natural Resour. Res. 16 (1), 31–43.

Gates, I.D., Adams, J., Larter, S., et al., 2008. The impact of oil viscosity heterogeneity on the production characteristics of tar sand and heavy oil reservoirs. Part II: Intelligent, geotailored recovery processes in compositionally graded reservoirs. J. Can. Pet. Technol. 47 (09).

Gearhart, M., Ziemer, K.A., Knight, O.M., 1981. Mud pulse MWD systems report. J. Pet. Technol. 33 (12), 2301–2306.

Germay, C., Denoël, V., Detournay, E., 2009a. Multiple mode analysis of the self-excited vibrations of rotary drilling systems. J. Sound Vib. 325 (1–2), 362–381. http://dx.doi.org/10.1016/j.jsv.2009.03.017, URL: http://linkinghub.elsevier.com/retrieve/pii/S0022460X09002478.

Germay, C., van de Wouw, N., Nijmeijer, H., Sepulchre, R., 2009b. Nonlinear drillstring dynamics analysis. SIAM J. Appl. Dyn. Syst. 8 (2), 527–553. http://dx.doi.org/10.1137/060675848, URL: http://epubs.siam.org/doi/abs/10.1137/060675848.

Godbey, J.K., 1967. Logging-while-drilling system. Google Patents, US Patent 3,309,656.

Gotawala, D.R., Gates, I.D., 2010. On the impact of permeability heterogeneity on SAGD steam chamber growth. Natural Resour. Res. 19 (2), 151–164.

Gray, S.H., Etgen, J., Dellinger, J., Whitmore, D., 2001. Seismic migration problems and solutions. Geophysics 66 (5), 1622–1640.

Greenberg, J., 2008. Seismic while drilling keeps bit turning to right while acquiring key real-time data. Drill. Contract. 64 (2), 44–45.

Guo, K., Li, H., Yu, Z., 2016. In-situ heavy and extra-heavy oil recovery: A review. Fuel 185, 886–902.

Halsey, G.W., Kyllingstad, A., Aarrestad, T.V., Lysne, D., 1986. Drillstring vibrations: Comparison between theory and experiments on a full-scale research drilling rig. In: SPE/IADC Drilling Conference, IADC/SPE 14760. Society of Petroleum Engineers, pp. 311–321. http://dx.doi.org/10.2118/14760-MS, URL: http://www.onepetro.org/doi/10.2118/14760-MS.

Hardage, B.A., et al., 1985. Vertical Seismic Profiling, vol. 14. Geophysical Press London.

Heim, W., Wolf, F.J., Savery, W.T., 1984. Heavy oil recovering. Google Patents US Patent 4,456,065.

Hubbard, S.M., Smith, D.G., Nielsen, H., Leckie, D.A., Fustic, M., Spencer, R.J., Bloom, L., 2011. Seismic geomorphology and sedimentology of a tidally influenced river deposit, Lower Cretaceous Athabasca oil sands, Alberta, Canada. AAPG Bull. 95 (7), 1123–1145.

Jackson, R.G., 1976. Depositional model of point bars in the lower wabash river. J. Sediment. Res. 46 (3), 579–594.

Jansen, J.D., 1993. Nonlinear Dynamics of Oilwell Drillstrings (Ph.D. thesis). Delft University Press, URL: http://repository.tudelft.nl/assets/uuid:d205b287-bcdd-4b49-b12a-963d9b906dea/3me_jansen_19930616.PDF.

Kapitaniak, M., Hamaneh, V.V., Chávez, J.P., Nandakumar, K., Wiercigroch, M., 2015. Unveiling complexity of drill–string vibrations: Experiments and modelling. Int. J. Mech. Sci. 101, 324–337.

Kazemi, N., Sacchi, M.D., 2014. Sparse multichannel blind deconvolution. Geophysics 79 (5), V143–V152. http://dx.doi.org/10.1190/geo2013-0465.1.

Kazemi, N., Shor, R., Innanen, K., 2018a. Imaging with a seismic-while-drilling dataset. In: Proc. CSPG CSEG CWLS Conv., pp. 1–4.

Kazemi, N., Shor, R., Innanen, K., 2018b. Illumination compensation with seismic-while-drilling plus surface seismic imaging. In: 80th EAGE Conference and Exhibition 2018. http://dx.doi.org/10.3997/2214-4609.201800880.

Kriesels, P., Keultjes, W., Dumont, P., Huneidi, I., Owoeye, O., Hartmann, R., et al., 1999. Cost savings through an integrated approach to drillstring vibration control. In: SPE/IADC Middle East Drilling Technology Conference. Society of Petroleum Engineers.

Labrecque, P.A., Jensen, J.L., Hubbard, S.M., Nielsen, H., 2011. Sedimentology and stratigraphic architecture of a point bar deposit, Lower Cretaceous McMurray Formation, Alberta, Canada. Bull. Canad. Petrol. Geol. 59 (2), 147–171.

Leckie, D.A., Smith, D.G., 1992. Regional Setting, Evolution, and Depositional Cycles of the Western Canada Foreland Basin. AAPG Special Volumes.

Leine, R., Van Campen, D., Keultjes, W., 2002. Stick-slip whirl interaction in drillstring dynamics. J. Vib. Acoust. 124 (2), 209–220.

Lines, L.R., Schultz, A.K., Treitel, S., 1988. Cooperative inversion of geophysical data. Geophysics 53 (1), 8–20.

Mateeva, A., Lopez, J., Potters, H., Mestayer, J., Cox, B., Kiyashchenko, D., Wills, P., Grandi, S., Hornman, K., Kuvshinov, B., Berlang, W., Yang, Z., Detomo, R., 2014. Distributed acoustic sensing for reservoir monitoring with vertical seismic profiling. Geophys. Prospect. 62 (4), 679–692.

Maxwell, S.C., Rutledge, J., Jones, R., Fehler, M., 2010. Petroleum reservoir characterization using downhole microseismic monitoring. Geophysics 75 (5), 75A129–75A137.

Meehan, R., Miller, D., Haldorsen, J., Kamata, M., Underhill, B., 1993. Rekindling interest in seismic while drilling. Oilfield Rev. 5 (1), 4–13.

Meehan, R.J., Nutt, L., Dutta, N., Menzies, J., 1998. Drill bit seismic: A drilling optimization tool. In: IADC/SPE Drilling Conference. Society of Petroleum Engineers, Dallas, Texas, p. 14. http://dx.doi.org/10.2118/39312-MS.

Montgomery, J.B., O'Sullivan, F.M., 2017. Spatial variability of tight oil well productivity and the impact of technology. Appl. Energy 195, 344–355. http://dx.doi.org/10.1016/j.apenergy.2017.03.038, URL: http://www.sciencedirect.com/science/article/pii/S0306261917302611.

Nandakumar, K., Wiercigroch, M., 2013. Stability analysis of a state dependent delayed, coupled two DOF model of drill-string vibration. J. Sound Vib. 332 (10), 2575–2592. http://dx.doi.org/10.1016/j.jsv.2012.12.020, URL: http://linkinghub.elsevier.com/retrieve/pii/S0022460X1200987X.

Navarro-Lopez, E.M., Cort, D., (2007). Sliding-mode control of a multi-DOF oilwell drillstring with stick-slip oscillations. In: Proceedings of the 2007 American Control Conference, New York City, pp. 3837–3842.

Nejadi, S., Kazemi, N., Curkan, J.A., Auriol, J., Durkin, P.R., Hubbard, S.M., Innanen, K.A., Shor, R.J., Gates, I.D., et al., 2020. Look ahead of the bit while drilling: Potential impacts and challenges of acoustic seismic while drilling in the mcmurray formation. SPE J. http://dx.doi.org/doi:10.2118/199931-PA.

Patruyo, D., 2010. A Computer Model of a 3-Dimensional Point Bar System (Ph.D. thesis). University of Calgary.

Peacock, M., 2010. Athabasca oil sands: reservoir characterization and its impact on thermal and mining opportunities. Geol. Soc. Lond. Petrol. Geol. Conf. Ser. 7 (1), 1141–1150.

Poletto, F., 2005. Energy balance of a drill-bit seismic source, part 1: Rotary energy and radiation properties. Geophysics 70 (2), T13–T28. http://dx.doi.org/10.1190/1.1897038.

Poletto, F., Miranda, F., 2004. Seismic While Drilling: Fundamentals of Drill-Bit Seismic for Exploration, vol. 35. Elsevier.

Ramakrishnan, T.S., Thambynayagam, R.M., 1999. Real time monitoring and control of downhole reservoirs. Google Patents. US Patent 5,992,519.

Rector, III, J.W., Hardage, B.A., 1992. Radiation pattern and seismic waves generated by a working roller-cone drill bit. Geophysics 57 (10), 1319–1333.

Rector, III, J., Marion, B.P., 1991. The use of drill-bit energy as a downhole seismic source. Geophysics 56 (5), 628–634.

Richard, T., Germay, C., Detournay, E., 2004. Self-excited stick-slip oscillations of drill bits. C. R. Méc. 332 (8), 619–626. http://dx.doi.org/10.1016/j.crme.2004.01.016, URL: http://linkinghub.elsevier.com/retrieve/pii/S1631072104001135.

Rossi, G., Corubolo, P., Böhm, G., Dell'Aversana, P., Vesnaver, A., Poletto, F., Morandi, S., Ceragioli, E., 2001. Joint 3D inversion of SWD and surface seismic data. First Break 19 (8), 453–459.

Sagert, C., Di Meglio, F., Krstic, M., Rouchon, P., 2013. Backstepping and flatness approaches for stabilization of the stick-slip phenomenon for drilling. IFAC Proc. Vol. 46 (2), 779–784.

Saldivar, B., Mondié, S., Loiseau, J.J., Rasvan, V., 2011. Stick-slip oscillations in oillwell drilstrings: Distributed parameter and neutral type retarded model approaches. IFAC Proc. Vol. (IFAC-PapersOnline) 18 (Part 1), 284–289. http://dx.doi.org/10.3182/20110828-6-IT-1002.00084.

Saldivar, B., Mondié, S., Niculescu, S.-I., Mounier, H., Boussaada, I., 2016. A control oriented guided tour in oilwell drilling vibration modeling. Annu. Rev. Control 42, 100–113.

Serrarens, A.F.A., van de Molengraft, M.J.G., Kok, J.J., van den Steen, L., 1998. H-infinity control for suppressing stick-slip in oil well drillstrings. IEEE Control Syst. Mag. 18 (2), 19–30. http://dx.doi.org/10.1109/37.664652, URL: http://ieeexplore.ieee.org/lpdocs/epic03/wrapper.htm?arnumber=664652.

Shor, R.J., Dykstra, M.W., Hoffmann, O.J., Coming, M., 2015. For better or worse: Applications of the transfer matrix approach for analyzing axial and torsional vibration. In: SPE/IADC Drilling Conference and Exhibition. Society of Petroleum Engineers, London, England, UK, p. 24. http://dx.doi.org/10.2118/173121-MS.

Smith, D.G., Hubbard, S.M., Leckie, D.A., Fustic, M., 2009. Counter point bar deposits: lithofacies and reservoir significance in the meandering modern Peace River and ancient McMurray Formation, Alberta, Canada. Sedimentology 56 (6), 1655–1669.

Spanos, P., Chevallier, A., Politis, N.P., Payne, M.L., 2003. Oil and gas well drilling: a vibrations perspective. Shock Vib. Digest 35 (2), 85–103.

Strobl, R.S., Wightman, D.M., Muwais, W.K., Cotterill, D.K., Yuan, L., 1997. Geological modelling of mcmurray formation reservoirs based on outcrop and subsurface analogues.

Su, Y., Wang, J., Gates, I., 2013. SAGD Well orientation in point bar oil sand deposit affects performance. Eng. Geol. 157, 79–92.

Su, Y., Wang, J.J., Gates, I.D., 2014. Orientation of a pad of SAGD well pairs in an athabasca point bar deposit affects performance. Mar. Pet. Geol. 54, 37–46.

Tang, X., Wang, T., Patterson, D., 2002. Multipole acoustic logging-while-drilling. In: SEG Technical Program Expanded Abstracts 2002. Society of Exploration Geophysicists, pp. 364–367.

Thomas, R.G., Smith, D.G., Wood, J.M., Visser, J., Calverley-Range, E.A., Koster, E.H., 1987. Inclined heterolithic stratification-terminology, description, interpretation and significance. Sediment. Geol. 53 (1–2), 123–179.

Vasconcelos, I., Snieder, R., 2008. Interferometry by deconvolution: Part 2-theory for elastic waves and application to drill-bit seismic imaging. Geophysics 73 (3), S129–S141.

Wehunt, C.D., Burke, N.E., Noonan, S.G., Bard, T.R., 2003. Technical challenges for offshore heavy oil field developments. In: Offshore Technology Conference. Offshore Technology Conference, Houston, Texas, p. 13. http://dx.doi.org/10.4043/15281-MS.

Willis, B.J., Tang, H., 2010. Three-dimensional connectivity of point-bar deposits. J. Sediment. Res. 80 (5), 440–454.

Zhang, W., Youn, S., Doan, Q.T., et al., 2007. Understanding reservoir architectures and steam-chamber growth at christina lake, alberta, by using 4D seismic and crosswell seismic imaging. SPE Reserv. Eval. Eng. 10 (05), 446–452.

Zhao, D., Hovda, S., Sangesland, S., 2016. Abnormal down hole pressure variation by axial stick-slip of drillstring. J. Petrol. Sci. Eng. 145, 194–204. http://dx.doi.org/10.1016/j.petrol.2016.04.004, URL: http://dx.doi.org/10.1016/j.petrol.2016.04.004.